

Exceeding the Maximum Speed Limit of the Joint Angle for the Redundant Tendon-driven Structures of Musculoskeletal Humanoids

Kento Kawaharazuka¹, Yuya Koga¹, Kei Tsuzuki¹, Moritaka Onitsuka¹, Yuki Asano¹, Kei Okada¹, Koji Kawasaki², and Masayuki Inaba¹

Abstract—The musculoskeletal humanoid has various biomimetic benefits, and the redundant muscle arrangement is one of its most important characteristics. This redundancy can achieve fail-safe redundant actuation and variable stiffness control. However, there is a problem that the maximum joint angle velocity is limited by the slowest muscle among the redundant muscles. In this study, we propose two methods that can exceed the limited maximum joint angle velocity, and verify the effectiveness with actual robot experiments.

I. INTRODUCTION

The musculoskeletal humanoid [1]–[3] has many biomimetic benefits such as the radioulnar structure of the forearm [4], the flexible spine [5], and the scapula structure with a wide range of motion [6]. One of the most important characteristics among these benefits is redundant muscle arrangement. This enables fail-safe redundant actuation that can continuously move even if a few muscles are ruptured [7], [8], and variable stiffness control using the redundancy and nonlinear elastic elements [7], [9]. On the other hand, there is a problem that high internal muscle tension or slack of antagonistic muscles can occur due to the model error. To solve the problem, antagonist inhibition control [10], dynamic modification of antagonistic relationships [11], and muscle relaxation control [12] have been developed so far.

In this study, we handle a newly found problem of the redundant muscle arrangement. The maximum joint angle velocity is limited by the slowest muscle among the redundant muscles. We propose methods to exceed the limited maximum joint angle velocity and solve the problem. In other words, this becomes not a problem but a benefit, in which the robot can move faster than the limited joint angle velocity that we have thought was the maximum so far.

To increase the joint angle velocity, optimization methods by software [13] have been developed so far. However, these optimizations cannot make use of the hardware characteristics of musculoskeletal humanoids. Also, regarding the axis-driven robots with variable stiffness mechanism, velocity maximization methods using the hardware have been developed [14], [15]. In this study, we propose simple methods to exceed the limited maximum joint angle velocity by making use of the redundant tendon-driven characteristics.

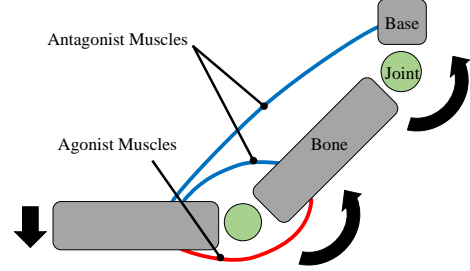


Fig. 1. The basic musculoskeletal structure.

This paper is organized as follows. In Section II, we will explain the basic musculoskeletal structure and its problem. In Section III, we will propose two simple methods to exceed the limited joint angle velocity. In Section IV, we will conduct experiments of two proposed methods using the musculoskeletal humanoid Musashi [3]. In Section V, we will compare the experimental results and discuss the advantages and disadvantages of these two methods.

II. MUSCULOSKELETAL HUMANOIDS

In this study, we generalize our explanation so that the complex musculoskeletal humanoids [1]–[3], in which the moment arms of muscles to joints are not constant, can be handled. The simple tendon-driven robots such as [16], [17] can also be handled. Although we assume that the muscle actuator is an electric motor, we can also apply the principle of this study to pneumatically actuated robots.

A. Basic Structure of the Musculoskeletal Humanoid

We show the basic musculoskeletal structure in Fig. 1. Muscles are antagonistically arranged around joints. The robot usually has not only monoarticular but also polyarticular muscles for the benefits of balancing and joint coordination [18]. We call the muscles contributing to the direction of the intended movement “agonist muscles,” and the muscles restraining the movement “antagonist muscles.” The relationship between joint angle and muscle length is represented as below,

$$l = h(\theta) \quad (1)$$

$$\Delta l = G(\theta)\Delta\theta \quad (2)$$

where l is muscle length, θ is joint angle, $\Delta\{l, \theta\}$ is a small displacement of $\{l, \theta\}$, h is a mapping from θ to l , and G is muscle Jacobian which is a differential matrix of h . Here, l is a m -dimensional vector and θ is a n -dimensional vector (m and n are the numbers of muscles and joints, respectively).

¹ The authors are with the Department of Mechano-Informatics, Graduate School of Information Science and Technology, The University of Tokyo, 7-3-1 Hongo, Bunkyo-ku, Tokyo, 113-8656, Japan. [kawaharazuka, koga, tsuzuki, onitsuka, asano, k-okada, inaba]@jsk.t.u-tokyo.ac.jp

² The author is associated with TOYOTA MOTOR CORPORATION. koji_kawasaki@mail.toyota.co.jp

B. Problem of the Redundant Tendon-driven Structure Addressed in This Study

As a movement with fast joint angle velocity, we consider the movement of swinging down the arm, such as striking the desk, hitting with a hammer, and swinging a golf club. We determine the joint angle θ^{start} when the arm is swung up, and the joint angle θ^{end} when swung down. If we represent the current joint angle as θ and the current joint angle velocity as $\dot{\theta}$ during the motion of swinging down the arm, the moment arms of muscles to joints \mathbf{r} are represented as below,

$$\mathbf{r}(\theta, \dot{\theta}) = G(\theta)\dot{\theta}/\|\dot{\theta}\|_2 \quad (3)$$

where $\|\cdot\|_2$ represents L2 norm. If \mathbf{r} of the muscle is positive, it is an antagonist muscle, and if \mathbf{r} of the muscle is negative, it is an agonist muscle. The absolute value of \mathbf{r} is the moment arm. If the muscle is a polyarticular muscle involving multiple joints or a muscle whose position is distant from joints, the moment arm becomes large. The larger the moment arm is, the faster the muscle length velocity must be, even with the same joint angle velocity. A muscle with a large moment arm can easily achieve the maximum muscle length velocity of the actuator limit \dot{l}^{limit} . Thus, the larger the index q as below is, the easier \dot{l}^{limit} is achieved.

$$q = \mathbf{r}((\theta^{start} + \theta^{end})/2, \theta^{end} - \theta^{start}) \oslash \dot{l}^{limit} \quad (4)$$

where \oslash is the element-wise division of the vector. q uses the muscle Jacobian at the center of θ^{start} and θ^{end} .

Also, muscles that can easily achieve \dot{l}^{limit} have another characteristic besides the large moment arms and the small \dot{l}^{limit} . When considering the movements with fast joint angle velocity, many movements such as hammer hitting, soccer, and golf use gravity. Thus, we move the body using not only the actuator output but also the effects of gravity and body inertia. We show the characteristics of such movements in Fig. 2 (this can be interpreted as the movement of the shoulder-elbow or hip-knee). In this situation, when comparing the moment arms, those of antagonist muscles are always larger than those of agonist muscles. This is because while antagonist muscles bridge the bones, agonist muscles pass along joints. Therefore, in the case of the same \dot{l}^{limit} , antagonist muscles are slower than agonist muscles, and the joint angle velocity is restrained even if agonist muscles move fast. If these antagonist muscles do not hinder the movement, the robot can move at the same speed as agonist muscles but also at a faster speed than the agonist muscles because of the effects of gravity and body inertia.

In addition, regarding agonist muscles, even if one of them is slower than the others, it does not restrain the movement of joints. This fact is always true, even though the situation of Fig. 2 does not occur when moving against gravity. Thus, the main cause limiting the joint angle velocity is the movement of antagonist muscles.

In this study, we focus on the management of antagonist muscles with large q so that they do not achieve \dot{l}^{limit} .

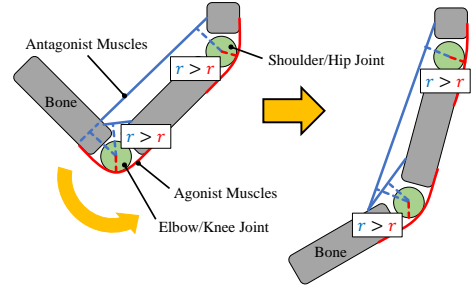


Fig. 2. Characteristics of movements with high joint velocity. These movements use the effect of gravity and body inertia.

III. A METHOD EXCEEDING THE LIMITED SPEED OF THE JOINT ANGLE

To solve the problem of Section II-B, we will propose two simple methods. The first one is a method inhibiting antagonist muscles with large q , thus making their current 0, and using backdrivability of muscles. The second one is a method elongating antagonist muscles with large q in advance.

A. Method Inhibiting Antagonist Muscles

This is a method not to manage the antagonist muscles but to inhibit them. This control is very simple, and the muscle motor current with large q is inhibited to 0 as below, soon after starting the movement,

$$o[i] = 0 \text{ if } q[i] > C \quad (5)$$

where i is the muscle index, o is the current of the motor, and C is a constant value. If $C = 0$, the currents of all the antagonist muscles become 0, and if $C > 0$, the currents of antagonist muscles with large moment arms and small \dot{l}^{limit} become 0. If the muscle actuators have backdrivability, the muscles spontaneously elongate when pulled, and we do not have to consider their maximum muscle length velocities. Because q gradually changes during the movement, this control runs at a high frequency. This method assumes that the muscle actuators have backdrivability, and we verify it later using the actual robot.

B. Method Elongating Antagonist Muscles

This is a method managing the maximum muscle velocity by elongating the antagonist muscles with large moment arms in advance. When choosing which muscle we should elongate, we must consider two points stated below.

First, when swinging up the arm or leg, the posture of θ^{start} must be achievable. Because antagonist muscles when swinging down are agonist muscles when swinging up, if we simply elongate them when swung up, the robot cannot achieve the posture of θ^{start} . Thus, when considering a mask \mathbf{m} whose values of muscles to elongate are 0 and those not to elongate are 1, the quadratic programming below must have a solution.

$$\begin{aligned} & \underset{\mathbf{f}}{\text{minimize}} && (\mathbf{m} \otimes \mathbf{f})^T W_1 (\mathbf{m} \otimes \mathbf{f}) \\ & \text{subject to} && \boldsymbol{\tau}^{nec} = -G^T(\theta^{start})(\mathbf{m} \otimes \mathbf{f}) \\ & && \mathbf{m} \otimes \mathbf{f}^{min} \leq \mathbf{m} \otimes \mathbf{f} \leq \mathbf{m} \otimes \mathbf{f}^{max} \end{aligned} \quad (6)$$

where \otimes is element-wise multiplication, \mathbf{f} is the calculated muscle tension, W_1 is a weight matrix (identity matrix in this study), τ^{nec} is a joint torque which is necessary to achieve θ^{start} , and $\mathbf{f}^{(min,max)}$ is a minimum or maximum muscle tension. If \mathbf{f} satisfying this condition can be calculated, θ^{start} is achievable, and the robot can elongate the muscles whose \mathbf{m} is 0 while keeping θ^{start} . This is a principle enabled by the muscle redundancy. Although elongating the muscles increases the muscle tension of the others, it is not a problem for a short time.

Second, by elongating the chosen antagonist muscles, the joint angle velocity must become faster. By determining \mathbf{m} and conducting a simulation as below, we can calculate the time cost to achieve θ^{start} to θ^{end} ,

$$\underset{\Delta\theta}{\text{minimize}} \quad (\theta^{end} - \theta - \Delta\theta)^T W_2 (\theta^{end} - \theta - \Delta\theta) \quad (7)$$

$$\text{subject to} \quad -\mathbf{m} \otimes \dot{l}^{limit} \Delta t \leq \mathbf{m} \otimes (G(\theta)\Delta\theta) \leq \mathbf{m} \otimes \dot{l}^{limit} \Delta t$$

where $\Delta\theta$ is the simulated displacement of the joint angle from θ , W_2 is a weight matrix (identity matrix in this study), t is the current time step, and Δt is the time interval of simulation. We can calculate $\Delta\theta$ representing how much θ can get closer to θ^{end} in Δt seconds. We update this simulation like $\theta \leftarrow \theta + \Delta\theta$ and $t \leftarrow t + \Delta t$, by starting from $\theta = \theta^{start}$. We stop the simulation when $\|\theta - \theta^{end}\|_2 < \epsilon$, and the last t is the time cost of the movement t^{cost} . We need to calculate \mathbf{m} that makes t^{cost} smaller. Although this calculation is a rough estimate because this simulation does not consider the motor inertia, model error, hysteresis, etc., we can obtain the rough characteristics of the movement. Because the musculoskeletal humanoid is difficult to modelize due to its complex structure compared with the ordinary axis-driven humanoid, we use such a simple method.

We search \mathbf{m} which can achieve θ^{start} by the calculated muscle tension and which makes t^{cost} smaller. Although we can conduct a full search of all the candidates of \mathbf{m} , t^{cost} clearly decreases when not using muscles with large q . Therefore, we make \mathbf{m} of antagonist muscles equal 0 in decreasing order of q , and stop the search when \mathbf{f} achieving θ^{start} no longer exists.

Finally, we calculate how long the muscles, whose \mathbf{m} are 0, should be elongated. We can obtain the transition of $\Delta\theta$ using a simulation conducted with the calculated \mathbf{m} . From the transition of joint angle, we can calculate the transition of muscle length using $G(\theta)\Delta\theta$. The maximum difference between the calculated muscle length transition and the fastest muscle length transition to elongate the muscles by \dot{l}^{limit} is $\Delta l^{elongate}$, which is the minimum amount of muscle length that should be elongated. By elongating the chosen muscles by $\Delta l^{elongate}$ at $\theta = \theta^{start}$ in advance, the antagonist muscles do not restrain the movement of agonist muscles, and the robot can move faster.

IV. EXPERIMENTS

A. Experimental Setup

In this study, we use the left arm of the musculoskeletal humanoid Musashi [3] for experiments. We show its muscle

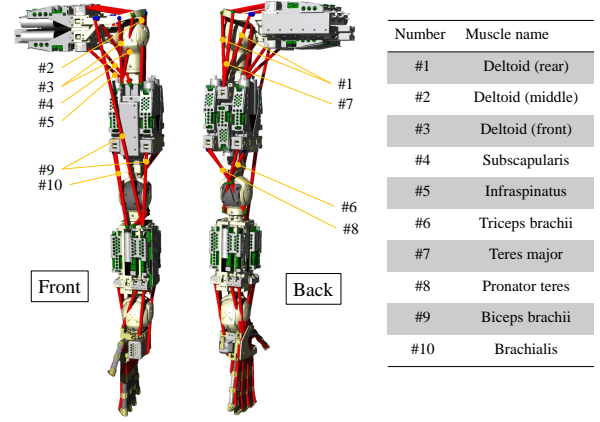


Fig. 3. Muscle arrangement of the left arm of the musculoskeletal humanoid Musashi [3].

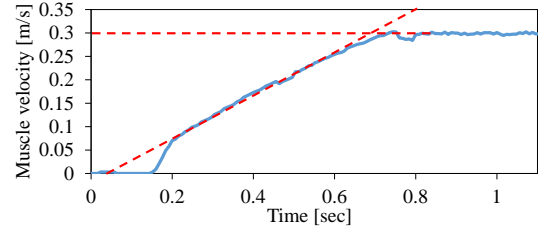


Fig. 4. Characteristics of muscle length velocity transition.

arrangement in Fig. 3. We mainly use its five DOFs of the shoulder and elbow. We represent these joint angles as S-p, S-r, S-y, E-p, E-y (S is the shoulder, E is the elbow, and rpy is roll, pitch, and yaw). These joints involve ten muscles including one polyarticular muscle. The motors of all the muscle actuators [19] are 90W Maxon BLDC Motor with 29:1 gear ratio, and \dot{l}^{limit} of them are the same. However, the current control in [19] cannot achieve \dot{l}^{limit} quickly. This is because the motor driver uses single-shunt approach to reduce the substrate size and we cannot increase the gain of current control to avoid the vibration of output. Therefore, we replace $-\dot{l}^{limit}$ and \dot{l}^{limit} in Eq. 7 by \dot{l}^{min} and \dot{l}^{max} , and we update them as below when the current muscle length velocity $\dot{l} > 0$,

$$\dot{l}^{max} = \min(\dot{l} + \alpha\Delta t, \dot{l}^{limit}) \quad (8)$$

$$\dot{l}^{min} = \min(\dot{l} - \alpha\Delta t, 0) \quad (9)$$

where α is a constant value. In this study, from Fig. 4, we identified that $\alpha = 0.46$ [m/s²] and $\dot{l}^{limit} = 0.30$ [m/s]. This is a constraint that while \dot{l} can gradually increase in proportion to time, \dot{l} can decrease to 0 at once. When $\dot{l} < 0$, the constraint is the same that \dot{l} can gradually decrease in proportion to time, and \dot{l} can increase to 0 at once. This expressed the behavior of actual muscle modules well.

In this study, we handle the movement of swinging down the left arm of Musashi. We show the experimental movements in simulation and in the actual robot, in Fig. 5. Although we cannot measure the joint angle of the ordinary musculoskeletal humanoid due to the complex joint structures, we can measure the joint angle of Musashi using the equipped joint modules. Also, we can measure muscle

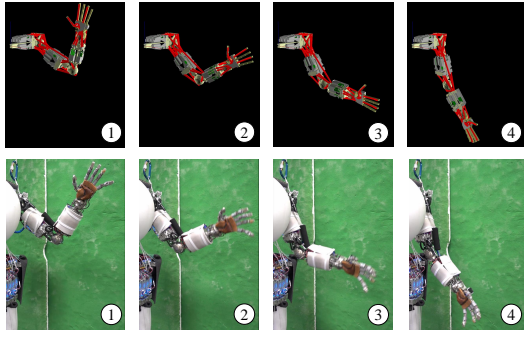


Fig. 5. Experimental motion of simulation and actual robot.

length from the encoder attached to the muscle actuator and muscle tension from the tension measurement unit. In this study, we set $C = 0$, $\Delta t = 0.03$, $f^{min} = 10$ [N], and $f^{max} = 200$ [N].

B. Basic Experiment

Before verifying the proposed methods, we conducted the target movement in simulation and in the actual robot without any proposed controls. Regarding all experiments, starting from θ^{start} , we sent the muscle length achieving θ^{end} for 0 seconds. First, we conducted the simulation method explained in the latter half of Section III-B. We set the mask \mathbf{m} as a vector whose elements are all 1. We show the transition of the joint angle velocity in Fig. 6. The maximum joint angle velocity was 2.4 rad/s of E-P, and t^{cost} was 0.99 seconds.

Second, we show the transition of joint angle velocity, muscle length velocity, and muscle tension when conducting the actual robot experiment, in Fig. 7. The maximum joint angle velocity was 2.6 rad/s of E-P, and the result was similar to the simulation. The muscle length velocities of the biceps brachii #9 and brachialis #10 achieved \dot{l}^{limit} . Also, the maximum muscle tension was about 290 N, and a heavy load was mainly applied to the agonist muscle of shoulder #1 and elbow #6. Regarding antagonist muscles, about 50 N was constantly applied to the polyarticular muscle of the biceps brachii #9.

C. Experiment with Method Inhibiting Antagonist Muscles

We conducted the target movement in simulation and in the actual robot with the method of Section III-A. First, we conducted a simulation by assuming that the robot has backdrivability and setting the mask \mathbf{m} as a vector whose elements of muscles with $q[i] > C$ (#2, #3, #9, #10) are 0 as explained in Eq. 5. We show the transition of the joint angle velocity in Fig. 8. The maximum joint angle velocity was 4.4 rad/s of E-P, and t^{cost} was 0.6 seconds.

Second, we show the transition of joint angle velocity, muscle length velocity, and muscle tension when conducting the actual robot experiment, in Fig. 9. The maximum joint angle velocity was 3.7 rad/s of E-P, and the observed velocity was lower than the simulation result. The muscle length velocities of the biceps brachii #9 and brachialis #10 were faster than \dot{l}^{limit} . Also, the maximum muscle tension was about 180 N, and a heavy load was mainly applied to the

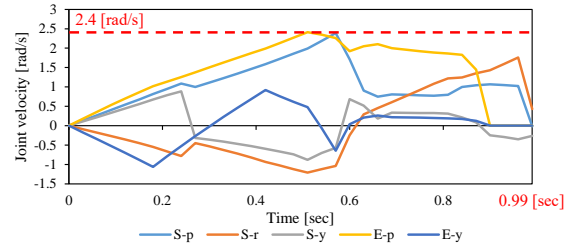


Fig. 6. Transition of joint angle velocity in simulation, without any proposed controls.

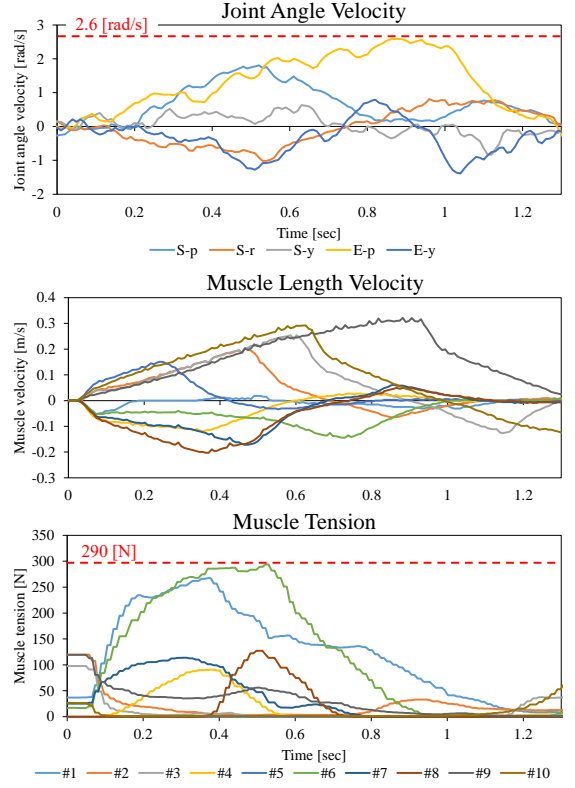


Fig. 7. Transition of joint angle velocity, muscle length velocity, and muscle tension in the actual robot, without any proposed controls.

agonist muscle of shoulder #1 and elbow #6. Regarding antagonist muscles, almost no muscle tension was observed.

D. Experiment with Method Elongating Antagonist Muscles

We conducted the target movement in simulation and in the actual robot with the method of Section III-B. First, we calculated the mask \mathbf{m} satisfying the conditions explained in Section III-B. Although the q of #9, #10, and #3 are large in decreasing order, if both #9 and #10 are elongated, the torque of the elbow cannot be kept. Therefore, we set \mathbf{m} as a vector whose element of only #9 is 0. We show the transition of joint angle velocity in Fig. 10. The maximum joint angle velocity was 3.3 rad/s of E-P, and t^{cost} was 0.78 seconds.

Second, we show the transition of the joint angle velocity, muscle length velocity, and muscle tension when conducting the actual robot experiment, in Fig. 11. The maximum joint angle velocity was 3.4 rad/s of E-P, and the result was similar to the simulation. The muscle length velocities of

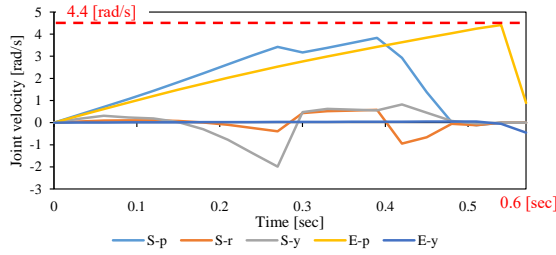


Fig. 8. Transition of joint angle velocity when using a method inhibiting antagonist muscles in simulation.

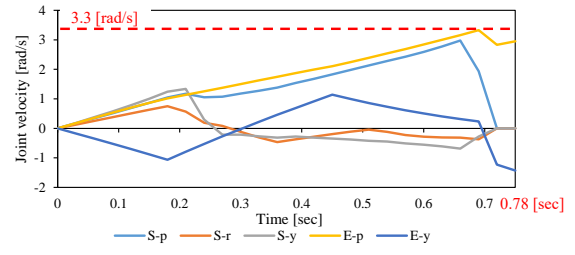


Fig. 10. Transition of joint angle velocity when using a method elongating antagonist muscles in simulation.

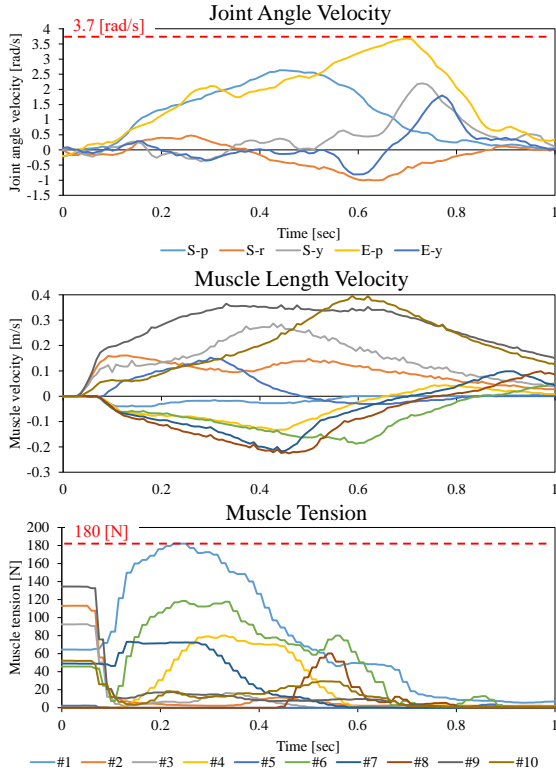


Fig. 9. Transition of joint angle velocity, muscle length velocity, and muscle tension when using a method inhibiting antagonist muscles in the actual robot.

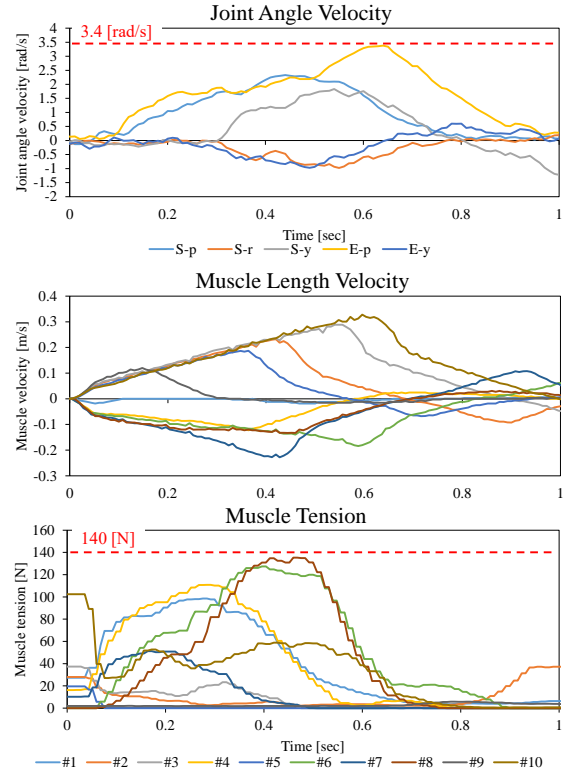


Fig. 11. Transition of joint angle velocity, muscle length velocity, and muscle tension when using a method elongating antagonist muscles in the actual robot.

the deltoid (front) #3 and brachialis #10 achieved \dot{l}_{limit} . Also, the maximum muscle tension was about 140 N, and a heavy load was mainly applied to the agonist muscles of elbow #6 and #8. Regarding antagonist muscles, about 60 N was constantly applied to the brachialis #10.

V. DISCUSSION

We show the comparison among the ordinary movement (**Basic**) and movements using the method of Section III-A (**Method-1**) or Section III-B (**Method-2**), in Table I. First, from the simulation results, the theoretical maximum joint angle velocity has the relationship of **Basic** < **Method-2** < **Method-1**. Also, the relationship of the actual robot experiments is the same with that of the simulation. Thus, the methods of this study are effective in maximizing joint angle velocity. However, regarding **Method-1**, there is a large error between the simulation and actual robot experiments. This is because **Method-1** is a method that assumes the muscle actuators have backdrivability. Although the gear ratio of

the muscle actuator is relatively low, 29:1, the joint angle velocity can decrease if we increase the gear ratio, due to the lack of backdrivability. Second, we consider the difference of muscle length velocities. Because **Method-1** makes the antagonist muscles elongate spontaneously, the muscle length velocity is higher than \dot{l}_{limit} . On the other hand, because **Method-2** elongates the antagonist muscles in advance, we cannot see the high muscle length velocity. Third, we consider the difference of muscle tensions. While large muscle tension emerges by large internal force regarding **Basic**, only about half of the muscle tension emerges regarding **Method-1** and **Method-2**. Thus, by inhibiting antagonist muscles or elongating them in advance, not only is joint angle velocity maximized but also muscle tension is reduced.

Summarizing the above, although **Method-1** is effective if the backdrivability is high, the performance can be worse than **Method-2** if the backdrivability is low. On the other hand, while the performance of **Method-2** is usually worse

TABLE I

COMPARISON AMONG THE BASIC MOTION (**BASIC**), THE MOTION WHEN USING THE METHOD OF SECTION III-A (**METHOD-1**), AND THE MOTION WHEN USING THE METHOD OF SECTION III-B (**METHOD-2**).

	Basic	Method-1	Method-2
Maximum $\dot{\theta}$ (simulation) [rad/s]	2.4	4.4	3.3
Maximum $\dot{\theta}$ (actual robot) [rad/s]	2.6	3.7	3.4
Maximum \dot{l} [m/s]	$\leq \dot{l}_{limit}$	$> \dot{l}_{limit}$	$\leq \dot{l}_{limit}$
Maximum T [N]	290	180	140

than that of **Method-1**, **Method-2** does not depend on the backdrivability. However, because **Method-2** elongates antagonist muscles in advance, high muscle tension is necessary when the joint angle is θ^{start} .

In this study, we developed simple methods exceeding the limited maximum joint angle velocity. By modeling the friction, hysteresis, and dynamics better, we can analyze the performance in more detail. In the future, we need to develop a method of realizing the accurate joint angle trajectory with fast velocity.

VI. CONCLUSION

In this study, we proposed two methods to exceed the maximum joint angle velocity limited by the actuator specifications for musculoskeletal humanoid robots with redundant tendon-driven structures. One of them is a method inhibiting antagonist muscles, thus making their current 0 and using backdrivability of muscles. Another one is a method elongating a few of the antagonist muscles in advance. From the simulation and actual robot experiments, we verified that the two methods can work well. Also, the performance of the former depends on the backdrivability, and that of the latter does not.

In future works, we would like to apply this method to more realistic situations.

REFERENCES

- [1] Y. Nakanishi, S. Ohta, T. Shirai, Y. Asano, T. Kozuki, Y. Kakehashi, H. Mizoguchi, T. Kurotobi, Y. Motegi, K. Sasabuchi, J. Urata, K. Okada, I. Mizuuchi, and M. Inaba, "Design Approach of Biologically-Inspired Musculoskeletal Humanoids," *International Journal of Advanced Robotic Systems*, vol. 10, no. 4, pp. 216–228, 2013.
- [2] M. Jäntschi, S. Wittmeier, K. Dalamagkidis, A. Panos, F. Volkart, and A. Knoll, "Anthrob - A Printed Anthropomorphic Robot," in *Proceedings of the 2013 IEEE-RAS International Conference on Humanoid Robots*, 2013, pp. 342–347.
- [3] K. Kawaharazuka, S. Makino, K. Tsuzuki, M. Onitsuka, Y. Nagamatsu, K. Shinjo, T. Makabe, Y. Asano, K. Okada, K. Kawasaki, and M. Inaba, "Component Modularized Design of Musculoskeletal Humanoid Platform Musashi to Investigate Learning Control Systems," in *Proceedings of the 2019 IEEE/RSJ International Conference on Intelligent Robots and Systems*, 2019, pp. 7294–7301.
- [4] K. Kawaharazuka, S. Makino, M. Kawamura, Y. Asano, Y. Kakiuchi, K. Okada, and M. Inaba, "Human Mimetic Forearm Design with Radioulnar Joint using Miniature Bone-muscle Modules and its Applications," in *Proceedings of the 2017 IEEE/RSJ International Conference on Intelligent Robots and Systems*, 2017, pp. 4956–4962.
- [5] M. Osada, T. Izawa, J. Urata, Y. Nakanishi, K. Okada, and M. Inaba, "Approach of "planar muscle" suitable for musculoskeletal humanoids, especially for their body trunk with spine having multiple vertebral," in *Proceedings of the 2011 IEEE-RAS International Conference on Humanoid Robots*, 2011, pp. 358–363.
- [6] Y. Sodeyama, T. Yoshikai, T. Nishino, I. Mizuuchi, and M. Inaba, "The Designs and Motions of a Shoulder Structure with a Wide Range of Movement Using Bladebone-Collarbone Structures," in *Proceedings of the 2007 IEEE/RSJ International Conference on Intelligent Robots and Systems*, 2007, pp. 3629–3634.
- [7] K. Kawaharazuka, K. Tsuzuki, S. Makino, M. Onitsuka, Y. Asano, K. Okada, K. Kawasaki, and M. Inaba, "Long-time Self-body Image Acquisition and its Application to the Control of Musculoskeletal Structures," *IEEE Robotics and Automation Letters*, vol. 4, no. 3, pp. 2965–2972, 2019.
- [8] K. Kawaharazuka, K. Tsuzuki, M. Onitsuka, Y. Asano, K. Okada, K. Kawasaki, and M. Inaba, "Musculoskeletal AutoEncoder: A Unified Online Acquisition Method of Intersensory Networks for State Estimation, Control, and Simulation of Musculoskeletal Humanoids," *IEEE Robotics and Automation Letters*, vol. 5, no. 2, pp. 2411–2418, 2020.
- [9] Y. Nakanishi, T. Izawa, M. Osada, N. Ito, S. Ohta, J. Urata, and M. Inaba, "Development of Musculoskeletal Humanoid Kenzoh with Mechanical Compliance Changeable Tendons by Nonlinear Spring Unit," in *Proceedings of the 2011 IEEE International Conference on Robotics and Biomimetics*, 2011, pp. 2384–2389.
- [10] K. Kawaharazuka, M. Kawamura, S. Makino, Y. Asano, K. Okada, and M. Inaba, "Antagonist Inhibition Control in Redundant Tendon-driven Structures Based on Human Reciprocal Innervation for Wide Range Limb Motion of Musculoskeletal Humanoids," *IEEE Robotics and Automation Letters*, vol. 2, no. 4, pp. 2119–2126, 2017.
- [11] Y. Koga, K. Kawaharazuka, M. Onitsuka, T. Makabe, K. Tsuzuki, Y. Omura, Y. Asano, K. Okada, and M. Inaba, "Modification of Muscle Antagonistic Relations and Hand Trajectory on the Dynamic Motion of Musculoskeletal Humanoid," in *Proceedings of the 2019 IEEE-RAS International Conference on Humanoid Robots*, 2019, pp. 632–637.
- [12] K. Kawaharazuka, K. Tsuzuki, M. Onitsuka, Y. Koga, Y. Omura, Y. Asano, K. Okada, K. Kawasaki, and M. Inaba, "Reflex-based Motion Strategy of Musculoskeletal Humanoids under Environmental Contact Using Muscle Relaxation Control," in *Proceedings of the 2019 IEEE-RAS International Conference on Humanoid Robots*, 2019, pp. 114–119.
- [13] R. Terasawa, S. Noda, K. Kojima, R. Koyama, F. Sugai, S. Nozawa, Y. Kakiuchi, K. Okada, and M. Inaba, "Achievement of Dynamic Tennis Swing Motion by Offline Motion Planning and Online Trajectory Modification Based on Optimization with a Humanoid Robot," in *Proceedings of the 2016 IEEE-RAS International Conference on Humanoid Robots*, 2016, pp. 1094–1100.
- [14] S. Haddadin, M. Weis, S. Wolf, and A. Albu-Schäffer, "Optimal Control for Maximizing Link Velocity of Robotic Variable Stiffness Joints," *IFAC Proceedings Volumes*, vol. 44, no. 1, pp. 6863–6871, 2011.
- [15] L. Chen, M. Garabini, M. Laffranchi, N. Kashiri, N. G. Tsagarakis, A. Bicchi, and D. G. Caldwell, "Optimal control for maximizing velocity of the CompAct compliant actuator," in *Proceedings of the 2013 IEEE International Conference on Robotics and Automation*, 2013, pp. 516–522.
- [16] S. Hirose and S. Ma, "Coupled tendon-driven multijoint manipulator," in *Proceedings of the 1991 IEEE International Conference on Robotics and Automation*, 1991, pp. 1268–1275.
- [17] H. Kobayashi, K. Hyodo, and D. Ogane, "On Tendon-Driven Robotic Mechanisms with Redundant Tendons," *The International Journal of Robotics Research*, vol. 17, no. 5, pp. 561–571, 1998.
- [18] M. A. Sharbafi, C. Rode, S. Kurowski, D. Scholz, R. Möckel, K. Radkhah, G. Zhao, A. M. Rashty, O. V. Stryk, and A. Seyfarth, "A new biarticular actuator design facilitates control of leg function in BioBiped3," *Bioinspiration & Biomimetics*, vol. 11, no. 4, p. 046003, 2016.
- [19] Y. Asano, T. Kozuki, S. Ookubo, K. Kawasaki, T. Shirai, K. Kimura, K. Okada, and M. Inaba, "A Sensor-driver Integrated Muscle Module with High-tension Measurability and Flexibility for Tendon-driven Robots," in *Proceedings of the 2015 IEEE/RSJ International Conference on Intelligent Robots and Systems*, 2015, pp. 5960–5965.